Research Article | Vol. 28, No. 23 / 9 November 2020 / Optics Express 34237
Optics EXPRESS

Plasmonic gold-cellulose nanofiber aerogels

QINGKUN LIU,[1,2] HARIDAS MUNDOOR,[1] GHADAH H. SHEETAH,[1,3,4] AND IVAN I. SMALYUKH[1,3,5,*]

[1]Department of Physics, Soft Materials Research Center and Department of Electrical, Computer, and Energy Engineering, University of Colorado, Boulder, CO 80309, USA
[2]Current address: School of Applied and Engineering Physics, Cornell University, Ithaca, NY 14850, USA
[3]Materials Science and Engineering Program, University of Colorado, Boulder, CO 80309, USA
[4]Current address: Department of Physics, King Faisal University, Hofuf 31982, Saudi Arabia
[5]Renewable and Sustainable Energy Institute, National Renewable Energy Laboratory and University of Colorado, Boulder, CO 80309, USA
*ivan.smalyukh@colorado.edu

Abstract: Assembly of plasmonic nanomaterials into a low refractive index medium, such as an aerogel, holds a great promise for optical metamaterials, optical sensors, and photothermal energy converters. However, conventional plasmonic aerogels are opaque and optically isotropic composites, impeding them from being used as low-loss or polarization-dependent optical materials. Here we demonstrate a plasmonic-cellulose nanofiber composite aerogel that comprises of well-dispersed gold nanorods within a cellulose nanofiber network. The cellulose aerogel host is highly transparent owing to the small scattering cross-section of the nanofibers and forms a nematic liquid crystalline medium with strong optical birefringence. We find that the longitudinal surface plasmon resonance peak of gold nanorods shows a dramatic shift when probed for the cellulose aerogel compared with the wet gels. Simulations reveal the shift of surface plasmon resonance peak with gel drying can be attributed to the change of the effective refractive index of the gels. This composite material may provide a platform for three- dimensional plasmonic devices ranging from optical sensors to metamaterials.

1. Introduction

Plasmonic nanomaterials, such as gold nanorods (GNRs), silver nanoprisms, play an important role in designing metamaterials, optical sensors, and photothermal energy converters [1–3]. Conventional plasmonic devices usually comprise metallic nanostructures on a solid surface or in a liquid medium [4,5], whose refractive indices are much larger than that of the air. However, aerogel, a synthetic highly porous material containing more than 95% of air, is of interest as a novel host medium to embed plasmonic nanomaterials. Dispersing plasmonic nanomaterials in an aerogel could enable three-dimensional systems which have low effective refractive index of the matrix and strong optical interaction of nanoparticles with the environment via the evanescent wave. Recent advances have demonstrated the plasmonic nanoparticles dispersed in inorganic or polymeric aerogel hosts, such as alumina, silica, and biomaterials [6–10]. Although these low-density aerogels exhibit excellent thermal insulation and a broad range of other interesting properties, the aerogel hosts are typically opaque and optically isotropic media owing to the non-negligible Mie scattering from the aerogels' isotropic network with large cross-section, impeding their application in optical devices which require low loss or polarization controllability.

To circumnutate these obstacles, one strategy is to embed plasmonic nanoparticles into aerogel hosts comprising nanometer-thin non-adsorptive fibers with well-controlled morphology, which could greatly reduce the scattering from the skeleton of the aerogel. A network of cellulose nanofibers (CNFs), each with a uniform cross-section of only 4-5 nm, is an ideal host material with low scattering [11–12]. CNFs could be readily prepared from abundant natural sources such as wood, cotton, and bacteria-produced cellulose. Furthermore, CNFs have a high aspect ratio of

#399181 https://doi.org/10.1364/OE.399181
Journal © 2020 Received 1 Jun 2020; revised 12 Oct 2020; accepted 12 Oct 2020; published 28 Oct 2020

Optics EXPRESS

~100-1000, which allows the nanofibers to form a nematic liquid crystal phase with an optical birefringence above a critical concentration [13].

Here we demonstrate a plasmonic gold-CNF composite aerogel that shows pronounced surface plasmon resonance (SPR) peaks at the resonance wavelengths and is highly transparent in the non-resonance regime. The GNRs with a polymeric capping are well-dispersed in the nanocellulose initially prepared colloidal host. The colloidal co-dispersion is then prompted to form a hydrogel via hydrogen bonds between the CNFs, followed by converting into alcogels via solvent exchange and being dried into aerogels. We find the longitudinal SPR (LSPR) peak of GNRs shows a dramatic blue shift in the aerogel as compared with wet gels. The aerogel host also has a tunable birefringence depending on the concentration of CNFs. We modeled the optical properties of the plasmonic gold-CNF gels by utilizing the discrete dipole approximation (DDA) method [14], which reproduced the experimental findings and revealed that the shift of surface plasmon resonance peak arises due to the change of the effective refractive index of the host medium and the CNF network enhances the light scattering efficiency of GNR particles embedded within the plasmonic gold-CNF aerogel.

2. Materials and methods

CNFs with the dimensions of 4.8 nm by several micrometers were synthesized by 2,2,6,6-tetramethylpiperidine-1-oxyl radical (TEMPO)–mediated oxidation of bleached softwood pulp [15]. Typically, 16 mg of TEMPO and 1.13 g of 80 wt.% sodium chlorite were dissolved in 0.05 M sodium phosphate buffer (90 mL) (pH 6.8) in a flask. A bleached softwood pulp (10 g, 10 wt.%) was suspended in the above solution. NaClO solution (455 mL) (13% active chlorine) was diluted 10 times with the same 0.05 M sodium phosphate buffer and added to the flask. The flask was stoppered, and the suspension was stirred at 500 rpm and 60 °C for 96 hours. After cooling the suspension to the room temperature, the TEMPO-oxidized celluloses were thoroughly washed with water by filtration. TEMPO-pretreated celluloses were then mechanically blended by a food processor (from Oster), homogenized by a sonifer (from Branson Ultrasonics), and filtered by a membrane filter. After oxidation, the electrostatic charging of the carboxylate anion on the surface of CNFs provides stabilization of the colloidal dispersions against aggregation in water.

GNRs were synthesized by the procedures described in detail in the literature [16,17]. To stabilize the GNRs in the acidic solution where the CNF dispersion is polymerized, we functionalized GNRs using thiol-terminated methoxy-poly(ethylene glycol) (mPEG-SH, JemKem Technology) following the literature [18]. For this, 1 mL of an aqueous solution with 30 mg of 5 kDa mPEG-SH was added to 50 mL of a diluted GNR dispersion with an optical density of 4. After stirring for 24 h, this dispersion was purified via centrifugation to eliminate the excess mPEG-SH.

Figure 1 illustrates the fabrication process of plasmonic gold -CNF gels. First, the PEG-capped GNRs with a concentration of 0.1-2.0 wt.% were mixed with the CNF aqueous solution. Since the PEG-capped GNRs are quite stable in CNF aqueous dispersion, the concentration of GNR could be further increased depending on the desired optical extinction. The CNFs were then cross-linked by prompting hydrogen bonds between carboxyl groups. This was achieved after adding several drops of hydrochloride acid, which transforms the CNF-GNRs aqueous dispersion into a hydrogel, as shown in Fig. 1(b). The hydrogel was then converted into an alcogel by exchanging the water with ethanol [Fig. 1(c)] and subsequently dried to an aerogel using critical point drying (CPD) [Fig. 1(d)].

Light transmittance spectra were obtained using a spectrometer (USB2000-FLG from Ocean Optics) mounted on an optical microscope (Olympus BX-51). Photographs of samples in the bright field mode and between crossed polarizers with a 530 nm retardation waveplate were taken using a digital camera. Transmission electron microscopy (TEM) images were obtained using a CM100 microscope (FEI Philips). The CNF samples were negatively stained with

Optics EXPRESS

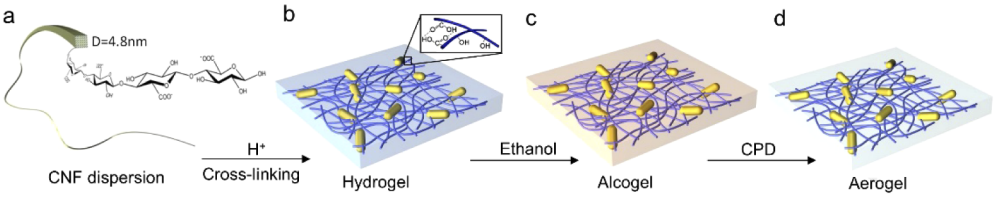

Fig. 1. Fabrication of a plasmonic gold-CNF aerogel. (a) The structure of CNFs initially obtained in an aqueous dispersion. (b) A hydrogel with interlinked CNFs was formed upon cross-linking of the individual fibers into a network. (c) An alcogel was obtained via the slow replacement of water with ethanol. (D) A plasmonic gold-CNF aerogel obtained by the drying of the alcogel using CPD.

phosphotungstic acid to increase imaging contrast. To achieve this staining, 2 µL of the sample was drop-casted on the TEM grid, allowed to settle for drying and then dipped into the stain solution (aqueous 2 wt% phosphotungstic acid). The plasmonic gold-CNF aerogels were characterized by utilizing scanning electron microscopy (SEM) using a Carl Zeiss EVO MA 10 system. For this, freshly cut surfaces of the plasmonic gold-CNF aerogels were sputtered with a thin layer of gold and observed under SEM at a low voltage of 5 kV.

The optical properties of plasmonic gold -CNF aerogel and GNR particles in different solvent media were computer-simulated using the DDA method [14,19–24], with the help of an online tool available at nanohub.org [24]. Three-dimensional structures of GNRs and rod-like CNFs were generated using a 3D drawing software (Blender v:2.75) and converted to a set of dipoles using the shape conversion tool, before importing into the nanoDDSCAT for numerical simulations. We simulated the light extinction, scattering efficiency factor, and the distributions of the magnitude of the electric field (|E|) around GNR particles, assuming an unpolarized beam of incident light.

3. Results and discussion

The mesoscale morphology of plasmonic gold-CNF aerogels was characterized by electron microscopy imaging (Fig. 2). TEM images show that the average dimensions of the used GNRs are 22 nm × 52 nm, 24 nm × 66 nm, and 31 nm × 94 nm, respectively [Figs. 2(a)–2(c)]. The CNFs have a uniform diameter of 4.8 nm and a typical length of several micrometers, as shown in Fig. 2(d). After the gelation, the CNF aerogel exhibits uniform three-dimensional network-like structures without aggregation or clustering. SEM images show the well-dispersed GNRs in the network of a CNF aerogel [Figs. 2(e) and 2(f)]. The GNRs orient randomly within the porous CNF network. For the provided example, the bulk density ρ_b is calculated to be 25 mg/cm^3 by the weight/volume ratio of the sample. The porosity, defined as $\varepsilon = (1\text{-}\rho_b/\rho_s)\times 100\%$, is then determined to be $\varepsilon \approx 98\%$ for the used aerogels, where ρ_s is the skeletal density, taken to be 1.5 g/cm^3.

The CNF gels provide a highly transparent monolithic host media for plasmonic nanomaterials. Figures 3(a)–3(c) show the pure CNF hydrogel transforms into alcogel via solvent exchange with ethanol, followed by converting into aerogel. When incorporated with gold nanorods, the hydrogels exhibit color similar to that observed before gelation, indicating the aggregation-free dispersion of the nanoparticles during the gelation process. When the wet gel is dried, the LSPR peak exhibits a remarkably strong blue shift compared with that in wet gels due to the distinct refractive indices of air and the solvents. The shift of extinction peak associated with LSPR is visualized in the change of appearance of the gels [Figs. 3(d)–3(f)]. The hydrogel and alcogel show brown color due to the extinction peaks at 500 nm and 700 nm. However, the aerogels show green color due to the large shift of the LSPR peak from 700 nm to 600 nm [Fig. 3(g)]. Differently from its longitudinal counterpart, the transverse SPR (TSPR) peak at ~530 nm is

Optics EXPRESS

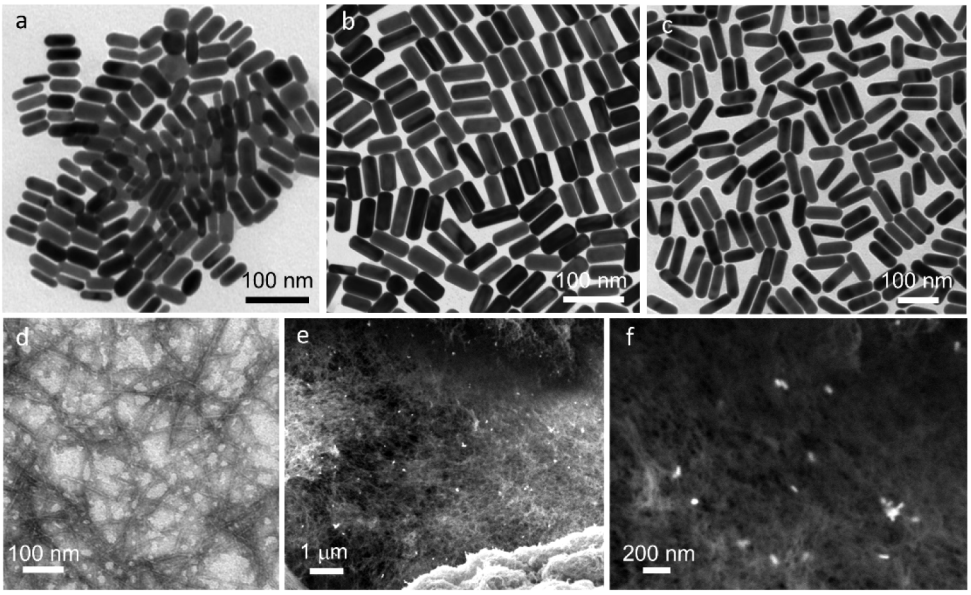

Fig. 2. Geometry of nanoparticles and mesoscale morphologies of plasmonic gold-CNF aerogels. (a-c) TEM images of gold nanorods with the average sizes of (a) 22 nm × 52 nm, (b) 24 nm × 66 nm, and (c) 31 nm × 94 nm. (d) TEM images of the negatively stained CNFs (e) Low- and (f) high-magnification SEM images of plasmonic gold-CNF aerogels featuring well-dispersed, individualized gold nanorods within the porous network.

not very sensitive to the change of the refractive index with the change and removal of the solvent. The numerical simulations also confirm the large shift of LSPR peak of aerogels from wet gels [Fig. 3(h)]. In Table 1, we summarize the particle size, TSPR, and LSPR peak positions of different GNRs used in the preparation of wet gels and aerogels. We also notice that the plasmonic gold-CNF aerogel shows a comparably large extinction at a shorter wavelength relative to those in wet gels. We attribute this to the scattering from the CNFs, which is considered in the numerical simulations illustrated in Fig. 4.

Table 1. Surface plasmon resonance peaks in plasmonic gold-CNF hydrogels, alcogels, and aerogels

Sample	LSPR peak (nm)			TSPR peak (nm)		
	hydrogel	alcogel	aerogel	hydrogel	alcogel	aerogel
Sample 1	629	634	566	516	519	505
Sample 2	646	652	587	518	520	514
Sample 3	700	707	611	517	518	507
Sample 4	752	764	653	514	516	505
Sample 5	785	794	658	518	519	508

To explain our experimental observations, we modeled the optical properties of plasmonic gold-CNF aerogel, assuming a simplified model of a rod-like CNF attached to the surface of a GNR particle. To account for the random alignment of CNF and GNR in the medium, the simulated spectra were averaged over different orientations of this geometry relative to the incident light's polarization as well as GNR orientations relative to the long axis of the CNF. In Figs. 4(a) and 4(b), we compare the extinction spectra and scattering efficiency factor of a

Optics EXPRESS

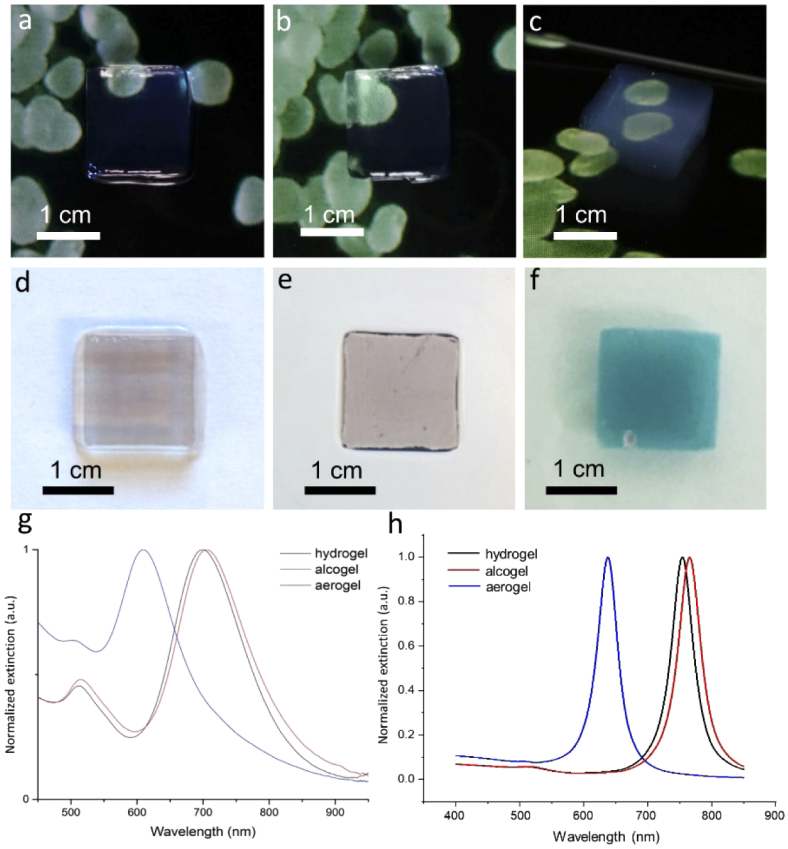

Fig. 3. Plasmonic gold-CNF gels. Highly transparent CNF (a) hydrogel, (b) alcogel, and (c) aerogel with slightly blueish hue due to Rayleigh scattering. Plasmonic gold-CNF (d) hydrogel, (e) alcogel, and (f) aerogel. (g) Experimental and (h) computer-simulated extinction spectra of the plasmonic gold-CNF hydrogel, alcogel, and aerogel.

CNF-attached GNR with that of a GNR particle in the air simulated based on the DDA method. The normalized extinction spectra of the CNF attached GNR particle indicates a slight red shift (~ 5 nm) in the LSPR peak [Fig. 4(a)] while showing significant enhancement in the scattering efficiency factor with respect to the same GNR particle in the vacuum or air [Fig. 4(b)]. The redshift in the LSPR peak of CNF attached GNR arises from the relatively higher refractive index of CNF compared to that of air. To analyze the enhanced scattering efficiency of the CNF attached GNR, we simulated the electric field distribution around the particles as depicted in Figs. 4(c)–4(f). Figures 4(c) and 4(e) show the electric field distribution near the surface of a CNF attached GNR for the incident wavelength of 520 nm and 580 nm, respectively, indicating the enhanced electric field intensity around the CNF, which corresponds to the increase in light scattering. The electric field distribution at the midplane of the GNR particle [Figs. 4(d) and 4(f)] shows the electric field enhancement due to the TSPR and LSPR modes of the GNR particles [2,3,19,20].

Depending on the concentration of CNF, the plasmonic gold-CNF gels exhibit a tunable optical birefringence, which allows for altering the polarization of incident light in plasmonic devices. The high length-to-width aspect ratio of CNFs (typically in the range from 300 to 500) assures the emergence of the lyotropic nematic liquid crystal phase behavior above the low critical concentration of ~1 vol.%, which is consistent with the Onsager theory [25]. When

Optics EXPRESS

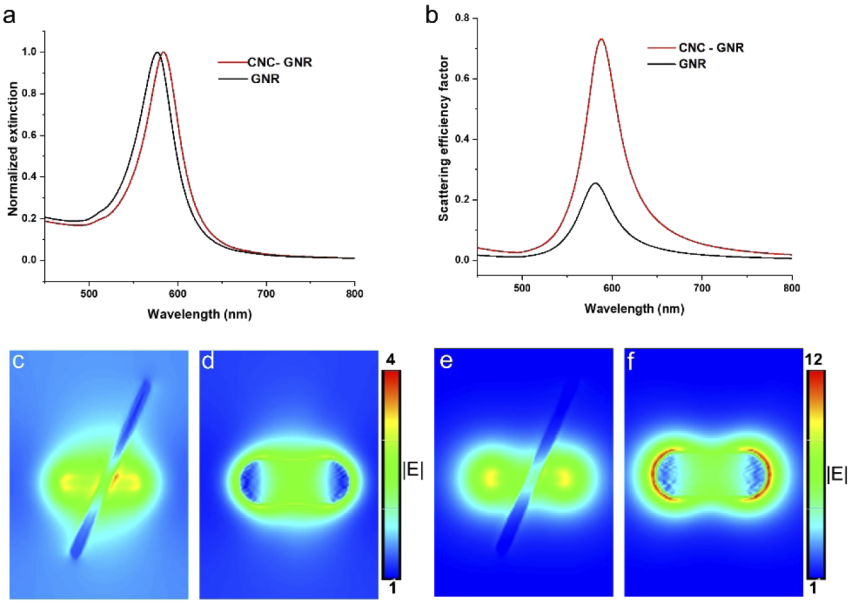

Fig. 4. Numerical simulations of light extinction, scattering, and electric field enhancement for a CNF-attached GNR particle. a,b) Simulated extinction spectra (a) and light scattering efficiency factor (b) of a GNR particle in the air attached to a rod-like CNF at the surface of the particle (red curve). The black curves in (a) and (b) represent the extinction spectra (a) and light scattering efficiency factor (b) of the same GNR particle without CNF. c,d) Electric field intensity map of a CNF attached GNR at an incident wavelength of 520 nm, showing the field enhancement at the surface (c) and midplane (d) of the particle owing to the TSPR mode of the GNR particle. e,f) Electric field intensity map of a CNF attached GNR at an incident wavelength of 580 nm, showing the field enhancement at the surface (e) and midplane (f) of the particle due to the LSPR mode of the GNR particle.

the concentration of CNF is below the critical concentration, the optically isotropic plasmonic gold-CNF aerogel could also be achieved. For example, when prepared using a low concentration of 0.1 wt.% of CNFs, the plasmonic gold-CNF hydrogel is optically isotropic except for a very weak birefringence at the edges induced by the strain during fabrication [Figs. 5(a)–5(c)]. When the concentration of CNFs is above the critical value, the CNFs readily form a nematic lyotropic liquid crystal. As shown in Figs. 5(d) and 5(f), an optically anisotropic hydrogel was prepared with the concentration of CNFs of 5 vol.%. The nematic order of CNFs is preserved in the plasmonic gold-CNFs aerogel when the gel is dried. Figures 5(h)–5(i) show an example of polarizing optical micrographs of a plasmonic gold-CNF aerogel [Fig. 2(g)] with 2 vol.% CNFs obtained under crossed polarizers before and after the insertion of a 530 nm retardation, respectively. This optical retardation $\Delta n_{eff} d$ is estimated to be of the order of the visible wavelength per millimeter of aerogel thickness d, based on the interference color, where Δn_{eff} is the effective optical anisotropy. This finding indicates that such aerogels can be used as polarizing optical elements for visible and infrared light. The optical retardation value could be tuned further by changing the concentration of CNFs and the thickness of the gels. Further future development could include unidirectional shearing of colloidal dispersions of CNFs before their cross-linking, which orients the CNFs and defines the orientation of the optical axis of the aerogels in the final product, as well as uniaxial and biaxial compression to define the ordering direction of both CNFs and GNRs. Importantly, such designs could either utilize the change of light polarization by the aerogel matrix through controlling Δn_{eff} for light traversing the aerogel in order to tune

Optics EXPRESS

how it interacts with gold nanoparticles, or, instead, this could be avoided by effectively working with more isotropic matrices at low densities of CNFs. Different wavelengths of light could be used to locally heat aerogels when matching the laser wavelength to that of TSPR or LSPR peaks or, instead, be transmitted. Such composite aerogel materials are of interest for various sensing applications.

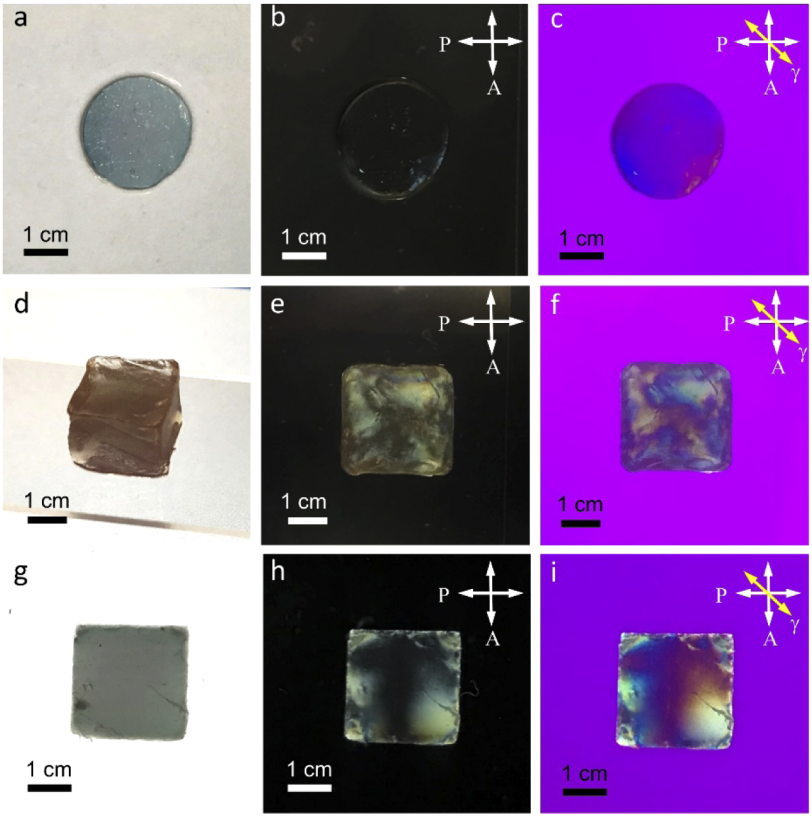

Fig. 5. Optically isotropic and anisotropic plasmonic gold-CNF gels. (a-c) photographs of a plasmonic gold-CNF hydrogel with 0.1 vol. % CNFs is optically isotropic except for a very weak strain-induced birefringence at the edges. (d-f) photographs of a plasmonic gold-CNF hydrogel with 5 vol.% CNF show a strong birefringence. (g-i) photographs of a plasmonic gold-CNF aerogel with 2 vol.% CNF reveal a strong birefringence. The corresponding polarized optical images obtained (b,e,h) before and (c,f,i) after the insertion of a 530 nm retardation plate, with a slow axis (γ) indicated by a yellow double-headed arrow.

4. Conclusion

We have demonstrated a plasmonic gold-CNF aerogel that comprises well-dispersed GNRs and nanometer-thin CNFs. The CNF-based gels serve as a highly transparent medium enabled by their ultrathin fiber network for assembling plasmonic nanoparticles. The plasmonic nanorods are randomly dispersed in the cellulose network, which could form both an optically isotropic medium and a nematic liquid crystal phase with a large birefringence, dependent on the concentration of CNFs. We observed a large blue shift in the LSPR peak of the plasmonic gold - CNF aerogel compared with the wet gels. Simulations reveal the shift of surface plasmon resonance peak is attributed to the change of the effective refractive index of the host and enhanced scattering

Optics EXPRESS

efficiency for the GNRs embedded within the CNF network. We believe our approach to assemble GNRs in a CNF aerogel could be further developed into an ordered system, in which the GNRs or CNFs could be aligned by shearing forces or magnetic fields within the initial colloidal dispersion, as well as by uniaxial and biaxial compression upon forming gels [26,27]. This new composite material could be used in optical sensors, electro-optic devices, three-dimensional optical metamaterials, etc. Our approach can be extended by combining plasmonic nanoparticles with other classes of nanomaterials through co-hybridizing them within either isotropic or nematic nanocellulose gels, with the interesting candidate nanoparticles ranging from quantum dots to carbon nanotubes and magnetic or photon-upconverting nanorods, potentially creating a paradigm for the fabrication of composite gels with pre-designable properties [28–30].

Funding

Advanced Research Projects Agency - Energy (DE-AR0000743).

Acknowledgments

We thank A. W. Frazier, J. A. De La Cruz, B. Senyuk, L. Jiang, and Y. Yuan for discussions and D. Rudman for technique assistance.

Disclosures

The authors declare no conflicts of interest.

References

1. S. Zouhdi, A. Sihvola, and A. P. Vinogradov, eds., *Metamaterials and plasmonics: fundamentals, modelling, applications* (Springer Science & Business Media, 2008).
2. M. E. Stewart, C. R. Anderton, L. B. Thompson, J. Maria, S. K. Gray, J. A. Rogers, and R. G. Nuzzo, "Nanostructured plasmonic sensors," Chem. Rev. **108**(2), 494–521 (2008).
3. X. Huang, P. K. Jain, I. H. El-Sayed, and M. A. El-Sayed, "Plasmonic photothermal therapy (PPTT) using gold nanoparticles," Lasers Med. Sci. **23**(3), 217–228 (2008).
4. J. Henzie, M. H. Lee, and T. W. Odom, "Multiscale patterning of plasmonic metamaterials," Nat. Nanotechnol. **2**(9), 549–554 (2007).
5. Q. Liu, Y. Cui, D. Gardner, X. Li, S. He, and I. I. Smalyukh, "Self-alignment of plasmonic gold nanorods in reconfigurable anisotropic fluids for tunable bulk metamaterial applications," Nano Lett. **10**(4), 1347–1353 (2010).
6. B. Klemmed, L. V. Besteiro, A. Benad, M. Georgi, Z. Wang, A. Govorov, and A. Eychmüller, "Hybrid plasmonic–aerogel materials as optical superheaters with engineered resonances," Angew. Chem. **132**(4), 1713–1719 (2020).
7. Y. Chen, K. C. Ng, W. Yan, Y. Tang, and W. Cheng, "Ultra flexible plasmonic nanocomposite aerogel," RSC Adv. **1**(7), 1265–1270 (2011).
8. P. A. DeSario, J. J. Pietron, A. Dunkelberger, T. H. Brintlinger, O. Baturina, R. M. Stroud, J. C. Owrutsky, and D. R. Rolison, "Plasmonic aerogels as a three-dimensional nanoscale platform for solar fuel photocatalysis," Langmuir **33**(37), 9444–9454 (2017).
9. L. Tian, J. Luan, K. K. Liu, Q. Jiang, S. Tadepalli, M. K. Gupta, R. R. Naik, and S. Singamaneni, "Plasmonic biofoam: a versatile optically active materia," Nano Lett. **16**(1), 609–616 (2016).
10. A. J. Hess, A. J. Funk, Q. Liu, J. A. De La Cruz, G. H. Sheetah, B. Fleury, and I. I. Smalyukh, "Plasmonic metamaterial gels with spatially patterned orientational order via 3D Printing," ACS Omega **4**(24), 20558–20563 (2019).
11. Y. Kobayashi, T. Saito, and A. Isogai, "Aerogels with 3D ordered nanofiber skeletons of liquid-crystalline nanocellulose derivatives as tough and transparent insulators," Angew. Chem. **53**(39), 10394–10397 (2014).
12. Q. Liu, A. W. Frazier, X. Zhao, J. A. De La Cruz, A. J. Hess, R. Yang, and I. I. Smalyukh, "Flexible transparent aerogels as window retrofitting films and optical elements with tunable birefringence," Nano Energy **48**, 266–274 (2018).
13. Q. Liu and I. I. Smalyukh, "Liquid crystalline cellulose-based nematogels," Sci. Adv. **3**(8), e1700981 (2017).
14. B. T. Draine and P. J. Flatau, "Discrete dipole approximation for scattering calculations," J. Opt. Soc. Am. A **11**(4), 1491–1499 (1994).
15. T. Saito, M. Hirota, N. Tamura, S. Kimura, H. Fukuzumi, L. Heux, and A. Isogai, "Individualization of nano-sized plant cellulose fibrils by direct surface carboxylation using TEMPO catalyst under neutral conditions," Biomacromolecules **10**(7), 1992–1996 (2009).

Optics EXPRESS

16. J. Perez-Juste, L. M. Liz-Marzan, S. Carnie, D. Y. C. Chan, and P. Mulvaney, "Electric-field-directed growth of gold nanorods in aqueous surfactant solutions," Adv. Funct. Mater. **14**(6), 571–579 (2004).
17. X. Ye, L. Jin, H. Caglayan, J. Chen, G. Xing, C. Zheng, V. DoanNguyen, Y. Kang, N. Engheta, C. R. Kagan, and C. B. Murray, "Improved size-tunable synthesis of monodisperse gold nanorods through the use of aromatic additives," ACS Nano **6**(3), 2804–2817 (2012).
18. Q. Liu, Y. Yuan, and I. I. Smalyukh, "Electrically and optically tunable plasmonic guest–host liquid crystals with long-range ordered nanoparticles," Nano Lett. **14**(7), 4071–4077 (2014).
19. H. Mundoor, G. H. Sheetah, S. Park, P. J. Ackerman, I. I. Smalyukh, and J. van de Lagemaat, "Tuning and switching a plasmonic quantum dot "sandwich" in a nematic line defect," ACS Nano **12**(3), 2580–2590 (2018).
20. P. J. Ackerman, H. Mundoor, I. I. Smalyukh, and J. van de Lagemaat, "Plasmon–Exciton Interactions Probed Using Spatial Coentrapment of Nanoparticles by Topological Singularities," ACS Nano **9**(12), 12392–12400 (2015).
21. B. T. Draine and P. J. Flatau, "User Guide to the Discrete Dipole Approximation Code DDSCAT 7.3," arXiv:1305.6497 (2012).
22. B. T. Draine and P. J. Flatau, "Discrete-dipole approximation for periodic targets: theory and tests," J. Opt. Soc. Am. A **25**(11), 2693–2703 (2008).
23. B. T. Draine and P. J. Flatau, "Fast near-field calculations in the discrete dipole approximation for regular rectilinear grids," Opt. Express **20**(2), 1247–1252 (2012).
24. P. K. Jain, N. Sobh, J. Smith, A. N. Sobh, S. White, J. Faucheaux, and J. Feser, "nanoDDSCAT," (2019) https://nanohub.org/resources/dda.
25. L. Onsager, "The effects of shape on the interaction of colloidal particles," Ann. N. Y. Acad. Sci. **51**(4), 627–659 (1949).
26. S. Zhang, M. A. Greenfield, A. Mata, L. C. Palmer, R. Bitton, J. R. Mantei, C. Aparicio, M. O. De La Cruz, and S. I. Stupp, "A self-assembly pathway to aligned monodomain gels," Nat. Mater. **9**(7), 594–601 (2010).
27. C. Wan, X. Chen, F. Lv, X. Chen, L. Meng, and L. Li, "Biaxial stretch-induced structural evolution of polyethylene gel films: Crystal melting recrystallization and tilting," Polymer **164**, 59–66 (2019).
28. N. Ould-Moussa, C. Blanc, C. Zamora-Ledezma, O. D. Lavrentovich, I. I. Smalyukh, M. F. Islam, A. G. Yodh, M. Maugey, P. Poulin, E. Anglaret, and M. Nobili, "Dispersion and orientation of single-walled carbon nanotubes in a chromonic liquid crystal," Liq. Cryst. **40**(12), 1628–1635 (2013).
29. H. Mundoor and I. I. Smalyukh, "Mesostructured composite materials with electrically tunable upconverting properties," Small **11**(41), 5572–5580 (2015).
30. Y. Li, Q. Liu, A. J. Hess, S. Mi, X. Liu, Z. Chen, Y. Xie, and I. I. Smalyukh, "Programmable ultralight magnets via orientational arrangement of ferromagnetic nanoparticles within aerogel hosts," ACS Nano **13**(12), 13875–13883 (2019).